Article

Cell Reports

Intravacuolar Membranes Regulate CD8 T Cell Recognition of Membrane-Bound *Toxoplasma gondii* Protective Antigen

Graphical Abstract

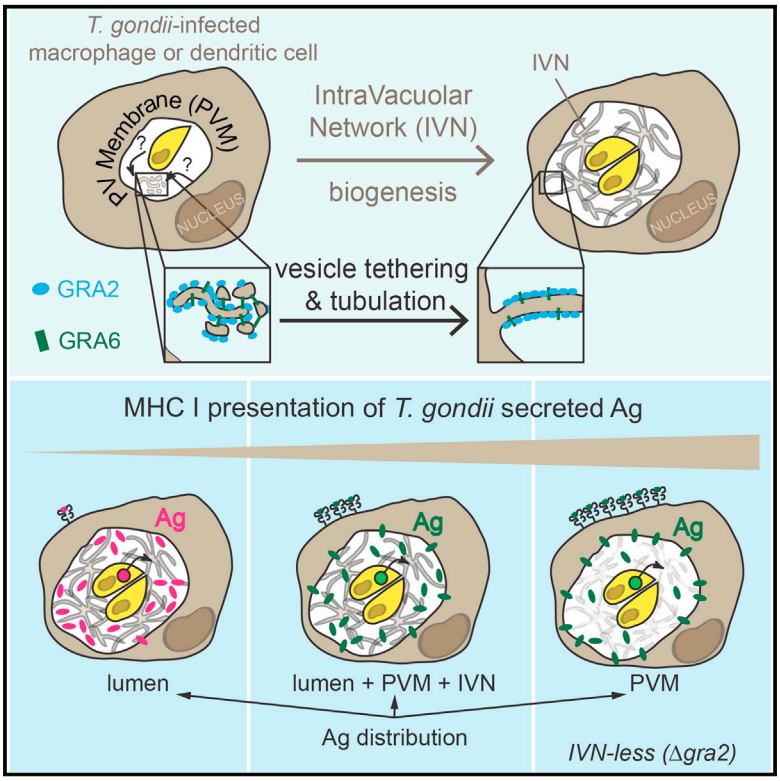

Highlights

- *T. gondii* GRA2 and GRA6 shape tubules of the intravacuolar network (IVN)
- GRA6 association with PV membranes promotes MHC I antigen presentation
- GRA6 binding to IVN limits its MHC I antigen presentation in vitro and in vivo
- Membranes of *T. gondii* IVN may play a role in immune modulation

Authors

Jodie Lopez, Amina Bittame, Céline Massera, ..., Corinne Mercier, Marie-France Cesbron-Delauw, Nicolas Blanchard

Correspondence

nicolas.blanchard@inserm.fr

In Brief

The host-*T. gondii* parasite interface comprises tubular membrane deformations. Lopez et al. clarify the function of parasite GRA2 and GRA6 effectors in tubule biogenesis and report that membrane-binding properties of parasite antigens influence their MHC I presentation by infected cells, suggesting that tubules may play an immune modulatory role.

Lopez et al., 2015, Cell Reports *13*, 2273–2286
December 15, 2015 ©2015 The Authors
http://dx.doi.org/10.1016/j.celrep.2015.11.001

Cell Reports
Article

Intravacuolar Membranes Regulate CD8 T Cell Recognition of Membrane-Bound *Toxoplasma gondii* Protective Antigen

Jodie Lopez,[1,2,3] Amina Bittame,[4,5] Céline Massera,[4,5] Virginie Vasseur,[1,2,3] Grégory Effantin,[6,7,8,9] Anne Valat,[4,5] Célia Buaillon,[1,2,3] Sophie Allart,[1,2,3] Barbara A. Fox,[10] Leah M. Rommereim,[10] David J. Bzik,[10] Guy Schoehn,[6,7,8,9] Winfried Weissenhorn,[6,7,8,9] Jean-François Dubremetz,[11] Jean Gagnon,[4,5] Corinne Mercier,[4,5] Marie-France Cesbron-Delauw,[4,5] and Nicolas Blanchard[1,2,3,*]
[1]INSERM, U1043, Toulouse 31300, France
[2]CNRS, UMR 5282, Toulouse 31300, France
[3]Centre de Physiopathologie de Toulouse Purpan (CPTP), Université de Toulouse, UPS, Toulouse 31300, France
[4]CNRS, UMR 5163, Grenoble 38000, France
[5]Laboratoire Adaptation et Pathogénie des Microorganismes (LAPM), Université Grenoble Alpes, Grenoble 38000, France
[6]Institut de Biologie Structurale (IBS), Université Grenoble Alpes, Grenoble 38044, France
[7]CNRS, IBS, Grenoble 38044, France
[8]CEA, IBS, Grenoble 38044, France
[9]CNRS, Unit for Virus Host-Cell Interactions (UVHCI), Grenoble 38042, France
[10]Department of Microbiology and Immunology, Geisel School of Medicine at Dartmouth, Lebanon, NH 03756, USA
[11]CNRS, UMR 5235, Université de Montpellier, Montpellier 34000, France
*Correspondence: nicolas.blanchard@inserm.fr
http://dx.doi.org/10.1016/j.celrep.2015.11.001

SUMMARY

Apicomplexa parasites such as *Toxoplasma gondii* target effectors to and across the boundary of their parasitophorous vacuole (PV), resulting in host cell subversion and potential presentation by MHC class I molecules for CD8 T cell recognition. The host-parasite interface comprises the PV limiting membrane and a highly curved, membranous intravacuolar network (IVN) of uncertain function. Here, using a cell-free minimal system, we dissect how membrane tubules are shaped by the parasite effectors GRA2 and GRA6. We show that membrane association regulates access of the GRA6 protective antigen to the MHC I pathway in infected cells. Although insertion of GRA6 in the PV membrane is key for immunogenicity, association of GRA6 with the IVN limits presentation and curtails GRA6-specific CD8 responses in mice. Thus, membrane deformations of the PV regulate access of antigens to the MHC class I pathway, and the IVN may play a role in immune modulation.

INTRODUCTION

The interplay between membrane proteins and their lipid environment is increasingly recognized as regulating many cellular processes (reviewed in Schmick and Bastiaens, 2014).

By providing the energy required for membrane deformation, the physical action of specialized proteins, such as those containing amphipathic alpha-helices (AAH), shapes membrane curvature (reviewed in Kozlov et al., 2014). Proteins containing AAH, in which the hydrophobic amino acids (aa) are located on one side of the helix while the polar, charged residues are located on the opposite side, typically insert into one monolayer leaflet. By virtue of interaction between the AAH positive charges and the lipid bilayer negative charges, membranes may be deformed into tubules (reviewed in Drin and Antonny, 2010).

Conversely, membrane curvature—and more extensively, the lipid environment (thickness, composition)—often dictate transmembrane protein structure and function. The lipid environment may influence translocation of molecules across membranes (Phillips et al., 2009). For example, membrane curvature affects the radius and permeability of pores made by the *Staphylococcus aureus* α-hemolysin toxin (Tonnesen et al., 2014). However, whether membrane deformations regulate molecular exchanges between an intracellular parasite and its host, thereby affecting host immune recognition of the parasite, remains unexplored.

Toxoplasma gondii (*T. gondii*) is an obligate intracellular parasite able to infect any warm-blooded animal. In humans, *T. gondii* is responsible for severe fetal abnormalities and for encephalitis in immunocompromised individuals. Following host cell invasion, *T. gondii* multiplies within a parasitophorous vacuole (PV) segregated from the cytosol by a limiting membrane. This membrane represents the major interface with the host cell. PV formation results from the sequential secretion of parasite secretory organelles called micronemes, rhoptries, and dense granules (Sibley, 2011). Although some of the rhoptry content is injected directly into the host cytosol upon initial contact, dense granule material is thought to be massively secreted at the time of vacuole formation and to be further exocytosed throughout the

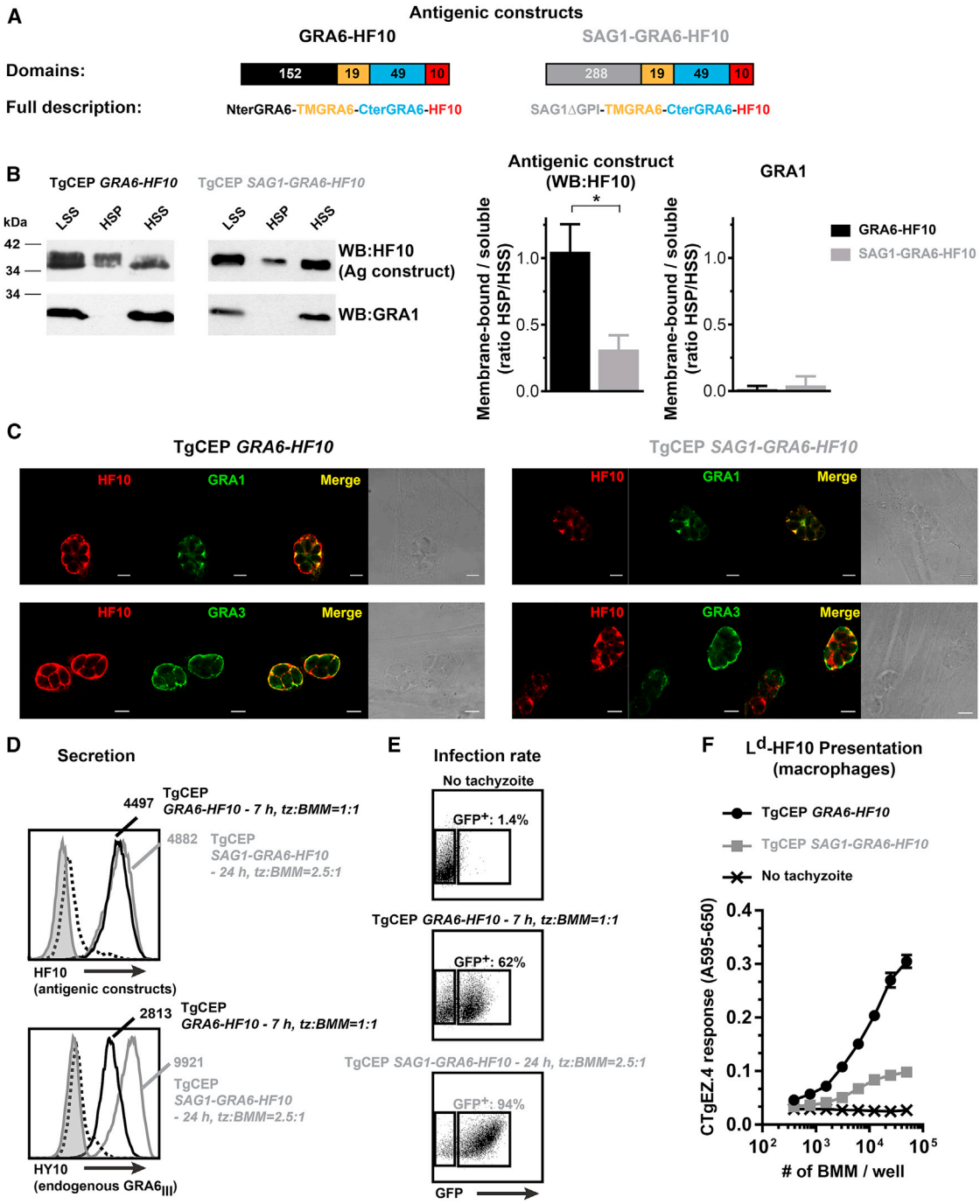

Figure 1. Association of the *T. gondii* Dominant Antigen GRA6 to Lipid Membranes of the PV Is Required for Efficient MHC I Presentation by Infected Macrophages

(A) Schematic representation of the two HF10-containing antigenic constructs transfected in TgCEP *GFP LUC*. GRA6-HF10 comprises the Nter $GRA6_I$-TM $GRA6_I$-Cter $GRA6_I$ (minus the last ten residues)-HF10 domains. SAG1-GRA6-HF10 comprises the SAG1 (minus glycosylphosphatidylinositol GPI)-TM $GRA6_I$-Cter $GRA6_I$ (minus the last ten residues)-HF10 domains. Numbers represent the size of each domain in aa.

(B) Solubility profile of GRA6-HF10 and SAG1-GRA6-HF10 in overnight-infected HFF after mechanical disruption and fractionation by low-speed and high-speed centrifugations. After elimination of the intact parasites and larger debris, the indicated antigenic (Ag) constructs present in the LSS, HSP (insoluble, membrane bound), or HSS (soluble) fractions were analyzed by western blot (WB) using anti-HF10 rabbit antiserum or anti-GRA1 mAb. Histograms show the mean ± SD of the HSP:HSS ratio, computed from three independent experiments.

(C) Subcellular localization of the GRA6-HF10 and SAG1-GRA6-HF10 antigenic constructs in 24-hr-infected HFF co-stained with anti-HF10 and anti-GRA1 (vacuolar lumen) or anti-GRA3 (PV membrane). Examples are representative of 20 PVs analyzed. Scale bar, 5 μm.

(legend continued on next page)

intracellular life of the parasite within its PV (Carruthers and Sibley, 1997; Leriche and Dubremetz, 1990). A prominent feature of the PV is the presence of an intravacuolar network (IVN), also referred to as the membranous nanotubular network, made of highly curved membrane tubules that connect the parasites together and to the PV membrane (Cesbron-Delauw et al., 2008; Sibley et al., 1995). We previously reported that two proteins secreted from the dense granules, GRA2 (Mercier et al., 2002; Travier et al., 2008) and GRA6 (Lecordier et al., 1995; Mercier et al., 2002), are implicated in IVN biogenesis. Shortly following their release into the vacuolar space, GRA2 and GRA6 localize to the posterior end of the parasite, where they associate with membrane whorls and vesicles that give rise to the IVN (Labruyere et al., 1999; Sibley et al., 1995). Deletion of the *GRA2* gene and complementation with truncated versions of GRA2 indicated that both its N-terminal domain and its three central AAH are necessary for IVN formation (Mercier et al., 2002; Travier et al., 2008). The N-terminal domain of GRA6 is crucial for association with the IVN (Gendrin et al., 2010), and, importantly, disruption of the *GRA6* gene led to replacement of the IVN by smaller tubules and vesicles (Mercier et al., 2002). These data suggested a model where GRA6 may help stabilize the membrane tubules initiated by GRA2 (Mercier et al., 2002). The IVN was initially proposed as a structural basis for ordered arrangement and synchronous division of the dividing parasites (Magno et al., 2005; Travier et al., 2008). The IVN may also be involved in virulence (Mercier et al., 1998) by helping to route parasite rhoptry effectors released in the host cytosol back to the PV membrane, thereby preventing PV destruction by immunity-related GTPases (Niedelman et al., 2012). More recently, the IVN has been implicated in the ingestion of host cytosolic material by the parasite (Dou et al., 2014). However, the exact molecular bases underlying IVN biogenesis as well as its function(s) remain ill defined.

Detection of *T. gondii* intrusion by CD8 T cells relies on the recognition of short antigenic peptides (8–10 aa) presented by major histocompatibility complex (MHC) class I (MHC I) molecules at the surface of infected cells. The generation of antigenic peptides from endogenous sources typically requires processing by cytosolic proteases, transport into the ER, trimming by ER-resident aminopeptidases, and loading onto peptide-receptive MHC I molecules (Blum et al., 2013). In the case of *T. gondii*, resistance to infection requires CD8 T cells (Parker et al., 1991; Suzuki and Remington, 1990), and MHC I processing is dependent on proteasome and TAP activity (Bertholet et al., 2006; Blanchard et al., 2008; Grover et al., 2014; Gubbels et al., 2005), suggesting that parasite antigenic precursors have to transit through the cytosol. Passage of *T. gondii* antigens to the cytosol may be facilitated by the recruitment of the host ER-associated degradation (ERAD) machinery onto the PV membrane (Cebrian et al., 2011; Goldszmid et al., 2009). However, the details of this export pathway remain elusive, and its mode of regulation has not been elucidated.

Here, we examined how membranes at the host-parasite interface that represent potential exit gates beyond the vacuolar space may regulate immunogenicity of *T. gondii* proteins. Using in vitro tubulation assays in a cell-free system, reverse genetics in *T. gondii*, and antigen presentation measurements, we report that insertion of a *T. gondii* dominant antigen (GRA6) at the PV membrane is key for immunogenicity. However, association of this antigen with the IVN limits its presentation and curtails the development of specific CD8 responses in mice.

RESULTS

Membrane Association of the *T. gondii* Antigen GRA6 Is Beneficial for MHC I Presentation

To determine the impact of protein binding to membranes on MHC I processing in parasite-infected cells, we set out to disturb the trafficking of a membrane-bound *T. gondii* antigen. We focused on the GRA6 antigen. In mice infected by type II *T. gondii*, GRA6 gives rise to a naturally processed decamer epitope (HPGSVNEFDF; namely, HF10), which is presented by MHC I L^d and elicits dominant and protective CD8 responses (Blanchard et al., 2008; Feliu et al., 2013). We chose to work with GRA6 because it is known to coexist as both a soluble form and a transmembrane form (Gendrin et al., 2010), inserted in membranes of the PV with a preferential IVN localization (Labruyere et al., 1999). Based on our previous observation that the N-terminal domain of GRA6 is responsible for its selective membrane association (Gendrin et al., 2010), we designed an antigenic construct bearing the HF10 epitope but comprising the SAG1 N-terminal domain instead of the natural GRA6 N-terminal domain (Figure 1A). This mutant was expected to behave mostly as a soluble protein within the vacuolar space. We stably transfected the control and mutant constructs into type III parasites (TgCEP *GFP LUC*, shortened here as TgCEP (see Table S1) (Feliu et al., 2013), which are naturally "HF10 null" due to polymorphisms in the GRA6 C-terminal domain. As expected, and despite the putative 19-residue transmembrane (TM) domain, biochemical fractionation of infected fibroblasts established that the antigenic construct bearing the SAG1 N-terminal domain was preferentially soluble, while the GRA6-HF10 control was equally distributed between the soluble and membrane fractions (Figure 1B). As a control, the purely soluble GRA1 protein (Sibley et al., 1995) was found exclusively in the high-speed supernatant (Figure 1B). These data were consistent with immunofluorescence analyses of the two antigenic constructs in combination with prototypical markers of the PV membrane (GRA3) and the PV lumen (GRA1). GRA6-HF10 was present both at the PV

(D) Upper panel: secretion level of GRA6-HF10 (black line) and SAG1-GRA6-HF10 (gray line) in BMM infected (GFP^+) with the indicated parasite line, for the indicated time and dose, detected with AF647-coupled anti-HF10. Lower panel: secretion level of endogenous $GRA6_{III}$ in BMM infected (GFP^+) with the indicated parasite line, detected with AF647-coupled anti-HY10. Controls show labelings of GFP^- cells from infected cultures (dotted lines) and BMM not mixed with tachyzoites (tinted histogram).

(E) Dot plots showing the proportion of GFP^+ BMM (i.e., infected cells) measured at the time of the antigen presentation assay.

(F) HF10 presentation by BMM infected in the same conditions as in (D) and (E), assessed with the CTgEZ.4 T cell hybridoma.

(D)–(F) are representative of two independent experiments with similar results.

membrane and in the PV lumen, most likely bound to the IVN, which cannot be resolved by light microscopy (Figure 1C, left panels). In contrast, the SAG1-GRA6-HF10 construct was mostly luminal and displayed limited overlap with the GRA3 PV membrane marker (Figure 1C, right panels).

When used to infect bone-marrow-derived macrophages (BMM), these two *T. gondii* lines revealed that HF10 presentation from the mostly soluble antigen (SAG1-GRA6-HF10) was dramatically reduced (Figure S1A). This difference could be attributed neither to impaired infectivity (Figure S1B) nor to defective expression of SAG1-GRA6-HF10 by tachyzoites, since it was actually ~3-fold more abundant than GRA6-HF10 (Figure S1C). As MHC I presentation of *T. gondii* antigens strongly relies on active secretion into the PV (Gregg et al., 2011), we sought to quantify the amount of GRA6 released into the PV by both parasite lines. To this aim, we designed a flow-cytometry-based assay that takes advantage of the fact that the saponin detergent permeabilizes both the host cell plasma membrane and the PV membrane, but not the intra-tachyzoite dense granules (Figures S1D–S1F). Thus, dense-granule-secreted material present within the host cell, but outside of the parasite, could be selectively quantified by flow cytometry. Using an anti-HF10 antibody, we consistently noticed a ~3-fold lower level of secretion of SAG1-GRA6-HF10 in infected macrophages (Figure S1G, upper panel). To explore the possibility that lower secretion of the mostly soluble antigen may explain its impaired presentation, we adjusted the infection conditions in order to obtain comparable levels of secretion of membrane-bound and soluble antigens (Figure 1D, top). To this aim, we reduced the dose and duration of infection with TgCEP *GRA6-HF10* tachyzoites (MOI, 1:1, 7 hr), as compared to TgCEP *SAG1-GRA6-HF10* tachyzoites (MOI, 2.5:1, 24 hr). Consequently, as expected, BMM incubated with TgCEP *GRA6-HF10* were infected at a lower rate (Figure 1E), and endogenous $GRA6_{III}$ was less abundant in the host cells (Figure 1D, bottom). However, MHC I presentation of the membrane-bound GRA6-HF10 antigen was still enhanced (Figure 1F). In conclusion, disrupting the association of a *T. gondii* dense granule antigen with vacuolar membranes impairs MHC I presentation by *T. gondii*-infected cells independently of the efficiency of dense granule secretion into the PV.

GRA2 Amphipathic α Helices, in Cooperation with GRA6, Deform Lipid Vesicles into Elongated Tubules, akin to Those of the IVN

Vacuolar membranes include the PV membrane and the IVN. To gain more insight into how these two membranous structures, that display different curvatures, could influence MHC I presentation, we sought to dissect how the tubules of the IVN are shaped. We had previously shown indirectly that IVN biogenesis requires GRA2 to initiate the membranous tubules of the IVN and GRA6 to stabilize them (Mercier et al., 2002). To establish the respective implications of each effector, we developed a minimal cell-free system to study the deformations of extruded large unilamellar vesicles (LUV) by recombinant GRA2 and/or GRA6. After characterizing the biophysical properties of the two recombinant proteins (Bittame et al., 2015), we analyzed the ability of rGRA2 or of a truncated rGRA2 mutant, from which the three AAH (rGRA2 ΔAAH) were deleted (Figure 2A), to bind to and deform LUV formed of lipids extracted from HeLa cells. Comparisons of LUV extruded at various diameters revealed that rGRA2 bound most efficiently to vesicles extruded at a 100-nm diameter (data not shown). The incubation products were then fractionated on a step gradient of sucrose. Iodine labeling revealed that the majority of the glycerophospholipid pool was present within the 0%–10% sucrose fractions (Figure 2B, upper panel). Even though a substantial amount of rGRA2 remained in the 30% and 40% sucrose fractions, indicative of protein aggregation, ~20% of the rGRA2 pool floated up to the 10% sucrose fraction, and some rGRA2 was detected in the 0% and 5% sucrose fractions (Figure 2B, middle panel). In contrast, rGRA2 ΔAAH was confined in the bottom 30%–40% sucrose fractions (Figure 2B, lower panel). These results were not the consequence of inherent rGRA2 ΔAAH instability, given that this protein folds in random coil (Bittame et al., 2015). Therefore, our data show that rGRA2 association with LUV depends on the domains of its AAH. Next, we evaluated the ability of rGRA2 to deform membranes by analyzing the LUV-protein incubation products by transmission electron microscopy (TEM). Tubules were detected at a lipid:protein ratio of 50:1, only when LUV were incubated with rGRA2 and not with rGRA2 ΔAAH (Figures 2C and 2D and S2A). In these conditions, the tubules were, on average, 178 ± 69 nm long, with a diameter of 25–33 nm (Table 1). As HeLa-extruded LUV have a complex lipid composition, we investigated whether the AAH of rGRA2 would exhibit selective affinity for particular membrane lipids. We incubated rGRA2 or rGRA2 ΔAAH with nitrocellulose membranes spotted with defined synthetic lipids (“fat blots”). Both proteins displayed similar intense reactivity with phosphatidylinositol (4)-monophosphate (PI(4)P), phosphatidylinositol (3,4,5)-trisphosphate ($PI(3,4,5)P_3$), and cardiolipin (CL), as well as similar weak reactivity with phosphatidylserine (PS). Only rGRA2 showed specific reactivity with phosphatidylinositol (4,5)-bisphosphate ($PI(4,5)P_2$) (Figure 2E). Accordingly, when rGRA2 was mixed with LUV of different (known or undetermined) lipid compositions; i.e., phosphatidylcholine (PC) + phosphatidylethanolamine (PE), PC + PE + $PI(4,5)P_2$ or total lipids extracted from HeLa cells, rGRA2 preferentially bound to HeLa LUV and LUV containing $PI(4,5)P_2$ (Figure S2B). These results indicate that (1) rGRA2 associates with 100-nm-diameter membrane vesicles through specific interactions between its AAH and $PI(4,5)P_2$ lipids, and (2) rGRA2 has the ability to deform these vesicles into membrane tubules, although the requirement for $PI(4,5)P_2$ in the tubulation process has not been investigated.

To explore the role of GRA6 in the tubulation process, we mixed recombinant GRA6 (rGRA6; Figure 3A) with HeLa LUV. We verified that rGRA6 could directly associate with the LUV (Figure 3B) and examined the incubation products by TEM. LUV incubated with rGRA6 appeared aggregated, but no tubule was observed (Figure 3C; Table 1). As a control, LUV incubated without rGRA6 were homogenously distributed on the grids (Figure 3C, right panel). These results suggest that rGRA6 may act by tethering membrane vesicles.

To examine the potential synergistic role of rGRA2 and rGRA6, we co-incubated 100-nm-diameter LUV with a mixture of rGRA2 and rGRA6 at a lipid:protein ratio of 50:1. Since the relative proportions of rGRA2 and rGRA6 in the PV are not known, we empirically

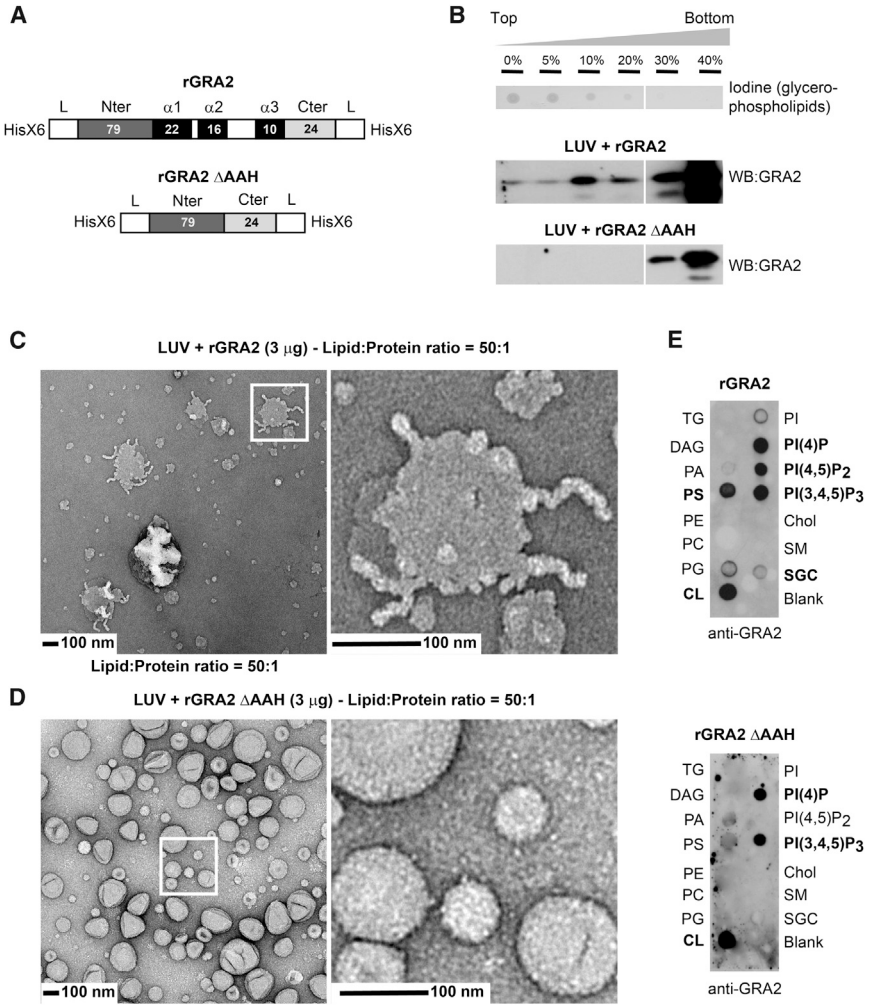

Figure 2. rGRA2 Induces Tubulation of Large Unilamellar Vesicles through Its Amphipathic α Helices, which Bind to PI(4,5)P_2 Lipids

(A) Schematic representation of the wild-type and AAH-deleted GRA2 recombinant proteins. The white boxes at both extremities indicate linkers (L), and numbers represent the size of each domain in aa. The recombinant proteins were tagged with polyhistidine residues at their N and C termini (Nter and Cter, respectively) (HisX6).

(B) Analysis of the incubation product of rGRA2 or rGRA2 ΔAAH with HeLa LUV extruded at 100 nm. Each protein was incubated with HeLa LUV at a lipid:protein ratio of 25:1. The binding mixture was mixed with 80% sucrose, loaded at the bottom of a tube, overlaid with a step sucrose gradient 40%–0% (bottom to top), and ultracentrifuged. Five microliters of each fraction was spotted onto nitrocellulose, and unsaturated phospholipids were revealed by fumigation with iodine (upper panel). An equal volume of each fraction was analyzed by western blot (WB) probed with anti-GRA2 mAb (middle and lower panels).

(C and D) TEM analysis of incubation products of rGRA2 (C) or rGRA2 ΔAAH (D) incubated with HeLa LUV extruded at 100 nm (lipid:protein, 50:1). A representative image is shown for each condition. The right image represents a magnified view of the area contained in the white box.

(E) Lipid-binding analysis of rGRA2 or rGRA2 ΔAAH by lipid-protein overlay. Recombinant proteins were incubated on lipid strips and probed with anti-GRA2 mAb. TG, triglyceride; DAG, diacylglycerol; PA, phosphatidic acid; PC, phosphatidylcholine; PG, phosphatidylglycerol; PI, phosphatidylinositol; Chol, cholesterol; SM, sphingomyelin; SGC, 3-sulfogalactosylceramide.

tested three different rGRA2:rGRA6 ratios. Both the 1:1 and the 25:1 ratios resulted in aggregated or coalescent LUV but not tubule (Figure S2C). By contrast, the 10:1 ratio led to ten times more abundant tubules than with rGRA2 alone, and tubules had a mean length of 150 ± 44 nm and a mean diameter of 20.7 ± 2.0 nm (Figure 3D; Table 1). Consistently, a more abundant fraction of rGRA2 floated up to the lightest sucrose fractions (0% and 5%) at the 10:1 ratio than at the 25:1 ratio (Figure S2D).

Taken together, these data suggest that there is a window of optimal rGRA2:rGRA6 proportions for tubule formation, and they support the notion that, by a process of vesicle tethering and tubulation, GRA6 and GRA2 are necessary and sufficient to deform vacuolar lipid vesicles into the elongated membranous tubules that constitute the IVN.

GRA2-Dependent IVN Biogenesis in Dendritic Cells and Macrophages

Knowing that membrane association positively regulates MHC I presentation of a membrane-bound antigen, we investigated how highly curved IVN membranes specifically impact this process. First, we selected the genetically amenable type I TgRH to assess the consequences of *GRA2* deletion on presentation of the GRA6-derived epitope. Since TgRH is naturally devoid of the HF10 epitope, we engineered this strain to express the GRA6-HF10 antigen using an existing GRA6(I)-deficient line (Mercier et al., 2002). The resulting parasites are referred to as TgRH *GRA6-HF10* for simplicity (Figure S3; Table S1). Then, we deleted *GRA2* by double-homologous recombination to obtain TgRH *GRA6-HF10* Δ*gra2* and generated the control complemented parasite TgRH *GRA6-HF10* Δ*gra2*/*GRA2*. Given that the IVN had been reported in fibroblasts but never in immune cells, we first examined the presence and shape of the IVN in parasite-infected, bone-marrow-derived dendritic cells (BMDC) by TEM. In BMDC infected with TgRH *GRA6-HF10* or the complemented TgRH *GRA6-HF10* Δ*gra2*/*GRA2*, membranous tubulovesicular material forming a network was observed within the PV lumen around the parasites (Figures S4A and S4C). In contrast, IVN tubular structures were absent from PVs containing GRA2-deficient parasites. In these PVs, only proteinaceous granular material was detected (Figure S4B). Similar observations were made using infected BMM (data not shown). Therefore, the IVN is also generated in a GRA2-dependent manner in professional antigen-presenting cells

Table 1. Influence of rGRA2 and rGRA6 on Tubule Number, Length, and Diameter

Conditions of LUV Incubation	No. of Fields Observed (1.8 μm^2/field)	Total Surface Counted (μm^2)	Total No. of Tubules	No. of Tubules/μm^2	Tubule Length (mean ± SD, in nm)	Range of Tubule Length (in nm)	Tubule Diameter (mean ± SD, in nm)
LUV only	13	42.1	0	0.0	NA	NA	NA
LUV + rGRA2	14	45.4	328	7.2	178 ± 69	90–350	28.8 ± 4.0
LUV + rGRA2 ΔAAH	14	45.4	16	0.4	ND	ND	ND
LUV + rGRA6	11	35.6	0	0.0	NA	NA	NA
LUV + rGRA2 + rGRA6	7	22.7	1,736	76.5	150 ± 44 (NS)	80–260	20.7 ± 2.0***

Quantifications were performed on HeLa LUV extruded at 100 nm and incubated at a lipid:protein ratio of 50:1. For rGRA2 + rGRA6 co-incubation, the rGRA2:rGRA6 ratio was 10:1. To compute the total number of tubules, tubules were enumerated from the indicated number of 1.8 μm^2 fields of view. Measurements of length and diameter were done on a sampling of 26 (rGRA2) and 28 (rGRA2 + rGRA6) straight tubules, selected from at least five different fields. p values were calculated with two-tailed non-parametric Mann-Whitney tests between the rGRA2 alone and the rGRA2 + rGRA6 condition. ***$p < 0.001$; NS, $p > 0.05$; ND, not determined; NA, not applicable.

(APC). These results establish a model to study the role of the IVN in MHC I presentation by infected APC.

The IVN Inhibits MHC I Presentation of the Membrane-Bound *T. gondii* Antigen GRA6

To interrogate the role of the IVN in MHC I presentation of the membrane-bound GRA6 antigen, we infected BMM in vitro with one of three parasite strains: TgRH *GRA6-HF10*, TgRH *GRA6-HF10* Δ*gra2*, or TgRH *GRA6-HF10* Δ*gra2/GRA2*. Despite similar infection rates (Figure 4A), HF10 presentation was enhanced by more than 8-fold when *GRA2* was deleted (Figure 4B). This was related neither to a difference in GRA6 expression by the transgenic parasites (Figure 4C) nor to a global increase in MHC I presentation capacity induced by TgRH *GRA6-HF10* Δ*gra2*, since presentation of an exogenously pulsed peptide, the SM9 peptide derived from the GRA4 antigen, was similar in all cases (Figure 4D). As GRA2 and GRA6 may (directly or indirectly) interact, absence of GRA2 could enhance secretion of GRA6 into the vacuolar space. Using the aforementioned "secretion assay," we found a slight (~20%) increase in the amount of vacuolar GRA6 in BMM infected with GRA2-deficient tachyzoites (Figure S5A). Adjustment of the infection conditions to equalize secretion (i.e., shorter infection time with TgRH *GRA6-HF10* Δ*gra2*) did not abolish the difference in HF10 presentation (Figure S5B), indicating that the IVN decreases presentation of the membrane-bound GRA6 independently from a potential effect on its secretion.

The availability of type II parasites deficient in non-homologous end joining, in which gene disruption is facilitated (Fox et al., 2011), then allowed us to address the role of GRA2 in the presentation of HF10 in its natural $GRA6_{II}$ context. Disruption of *GRA2* in TgPru Δ*ku80* increased presentation of the HF10 peptide by infected BMM (Figure 4E), while both the infection rate (Figure 4F) and the level of $GRA6_{II}$ protein expression (Figure 4G) were similar. Again, the modestly increased GRA6 secretion observed for TgPru Δ*gra2* was not responsible for enhanced HF10 presentation (Figure S5D).

Importantly, similar findings were made with BMDC, which constitute the most potent cell subset for priming parasite-specific CD8 T cells (Figures S5E–S5J).

Next, we questioned whether the increased MHC I presentation in the absence of GRA2 applies to all *T. gondii*-derived antigens, regardless of their membrane association properties. To this aim, we deleted *GRA2* in a parasite strain expressing the soluble SAG1-OVA model antigen (TgRH *YFP SAG1-OVA*) (Gubbels et al., 2005). Neither the amount of SAG1-OVA expressed by tachyzoites (Figure 4H) nor the infectivity of the parasites (Figure 4I) were affected by *GRA2* deletion. OVA-derived SL8 presentation by MHC I K^b was modestly increased (~2-fold) with GRA2-deficient parasites (Figure 4J), suggesting that the GRA2-mediated negative regulation of MHC I presentation by IVN membranes is selective, with a more pronounced effect for IVN membrane-associated antigens.

To strengthen the relevance of these findings, we next investigated the influence of the IVN on the expansion of CD8 T cell responses in vivo using a protocol of prime/boost immunization with irradiated tachyzoites, which can still generate the IVN (Figure 5A and S6A–S6D). Four days following the second immunization (i.e., at day 25), we assessed the magnitude of CD8 T cell responses to the dominant GRA6-derived HF10 peptide and the subdominant Tgd057-derived SVL8 peptide (Wilson et al., 2010) in the spleen (Figure 5B) and the peritoneum (Figure 5C). In comparison to GRA2-expressing parasites, TgRH *GRA6-HF10* Δ*gra2* elicited a significantly higher proportion of HF10-reactive CD8 T cells in both tissues examined, whereas no statistically significant difference was observed for the Tgd057-specific response. Subcellular fractionation showed that most of the Tgd057 protein was present in the soluble fraction (Figure 5D). Accordingly, immunofluorescence analyses revealed the presence of Tgd057 within the PV lumen, with limited overlap with GRA5, a marker of the PV membrane (Figure 5E). At last, enhanced HF10-specific CD8 responses were also detected when mice were injected with live TgPru tachyzoites deficient for *GRA2*, although interpretations are complicated by the dramatically reduced virulence of the TgPru Δ*gra2* (Figures S6E–S6G). In summary, our in vitro and in vivo data strongly suggest that membranes of the IVN negatively regulate MHC I presentation and CD8 T cell responses to membrane-bound *T. gondii* antigens.

Disruption of the IVN Increases GRA6 Targeting to the PV Membrane

Intriguingly, although membrane binding of the *T. gondii* antigen GRA6 was beneficial to its MHC I presentation, targeting to the IVN was detrimental. To understand this seemingly paradoxical result, we analyzed the subcellular localization and solubility

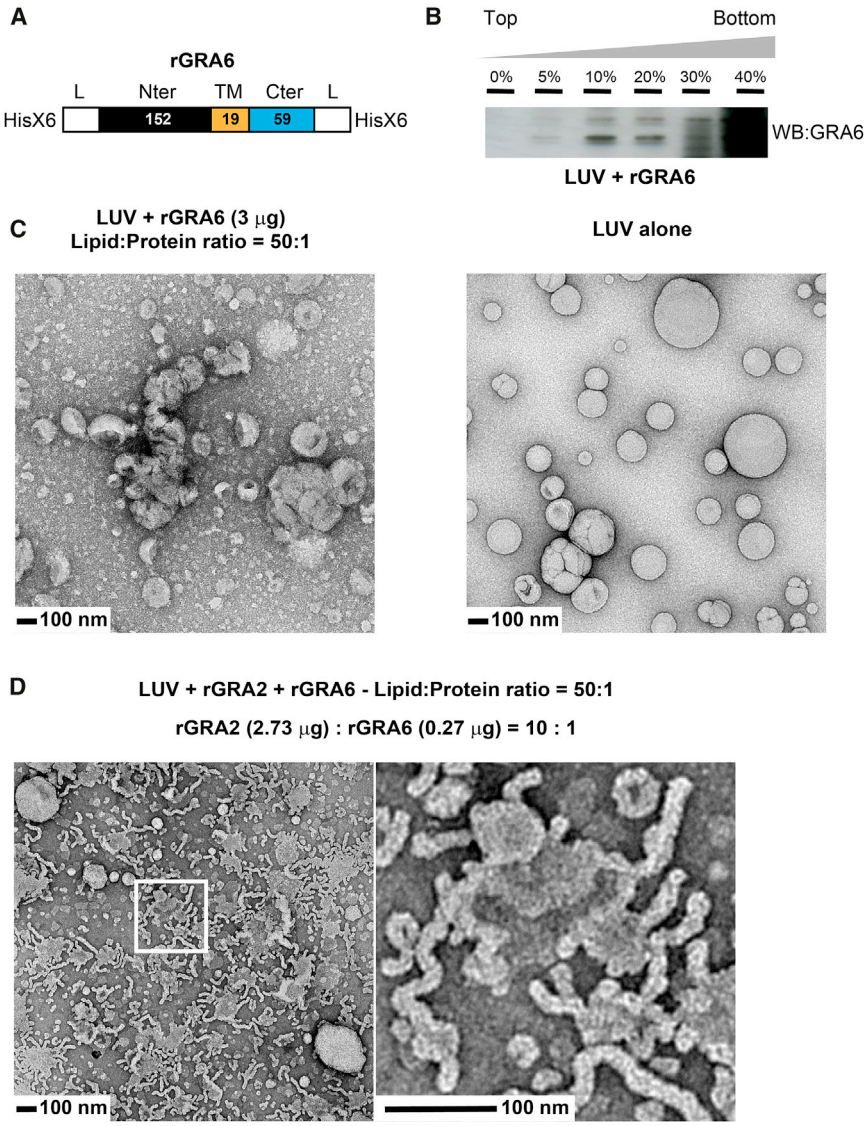

Figure 3. By Tethering Vesicles, rGRA6 Cooperates with rGRA2 to Deform Large Unilamellar Vesicles into Elongated Tubules akin to the Tubular IVN

(A) Schematic representation of the wild-type GRA6 recombinant protein. The white boxes at both extremities indicate linkers (L), and numbers represent the size of each domain in aa. The recombinant protein was tagged with polyhistidine residues at its N and C termini (Nter and Cter, respectively) (HisX6).

(B) Analysis of the incubation product of rGRA6 with HeLa LUV extruded at a 100-nm diameter, at a lipid:protein ratio of 50:1. Following fractionation on a step sucrose gradient 40%–0% (bottom to top), an equal volume of each fraction was analyzed by western blot (WB) probed with rabbit anti-GRA6 antiserum.

(C) TEM analysis of HeLa LUV extruded at a 100-nm diameter and incubated (left panel) or not (right panel) with rGRA6 at a lipid:protein ratio of 50:1.

(D) TEM analysis of the co-incubation of rGRA2 and rGRA6 with HeLa LUV extruded at 100 nm (lipid:protein, 50:1; rGRA2:rGRA6, 10:1). The right image represents a magnified view of the area contained in the white box. Representative images are shown.

profile of GRA6 in the presence or absence of the IVN. Biochemical fractionation revealed that the proportion of soluble GRA6 was not altered by the deletion of *GRA2* (Figure 6A). This largely unchanged solubility profile indicated that, in the absence of the IVN, GRA6 was likely targeted to other membranes of the PV, such as its limiting membrane. To test this hypothesis, we used confocal microscopy sections to quantify the fluorescence signal of GRA6-HF10 present in the vicinity of the PV membrane versus that contained in the entire PV (Figure 6B). Deletion of *GRA2* led to a preferential localization of GRA6 at the PV membrane (Figure 6C). Thus, enhanced access of the membrane-bound GRA6 antigen to the MHC I pathway correlates with its redistribution at the PV membrane.

DISCUSSION

As a means of subverting, persisting, and propagating to new hosts, intracellular protozoan parasites introduce many components into their host cells. A potential "side effect" is the processing of this material for presentation by MHC class I molecules, potentially resulting in immune detection by CD8 T cells. The *T. gondii*-secreted components can be soluble or membrane bound and have peculiar targeting locations including the highly curved membranes of the IVN; yet, how these membranes impact CD8 T cell responses was unexplored. Using a cell-free system to study IVN biogenesis, we showed that, by cooperatively binding to negatively charged lipids, GRA2 and GRA6 promote the formation of membrane tubules by a process of vesicle tethering (GRA6) and tubule formation (GRA2) (see the working model in Figure S7). In PV containing GRA2-deficient parasites (i.e., lacking the IVN to which GRA6 can bind), the membrane-bound GRA6 was "freed up" to relocate in larger proportion to the PV limiting membrane. We hypothesize that one consequence of this relocation is the enhancement of MHC class I presentation of GRA6. In summary, we demonstrate that the binding mode of a *T. gondii* antigen to membranes largely determines MHC class I presentation by infected cells and the development of CD8 T cell responses.

The significance of this work is at least 3-fold. First, our data suggest that the IVN may play an immune modulatory role by interfering with MHC class I processing of membrane-bound vacuolar antigens. This adds a new potential function to the already described roles for the IVN, such as host material uptake (Dou et al., 2014) or intra-PV tachyzoite organization (Travier

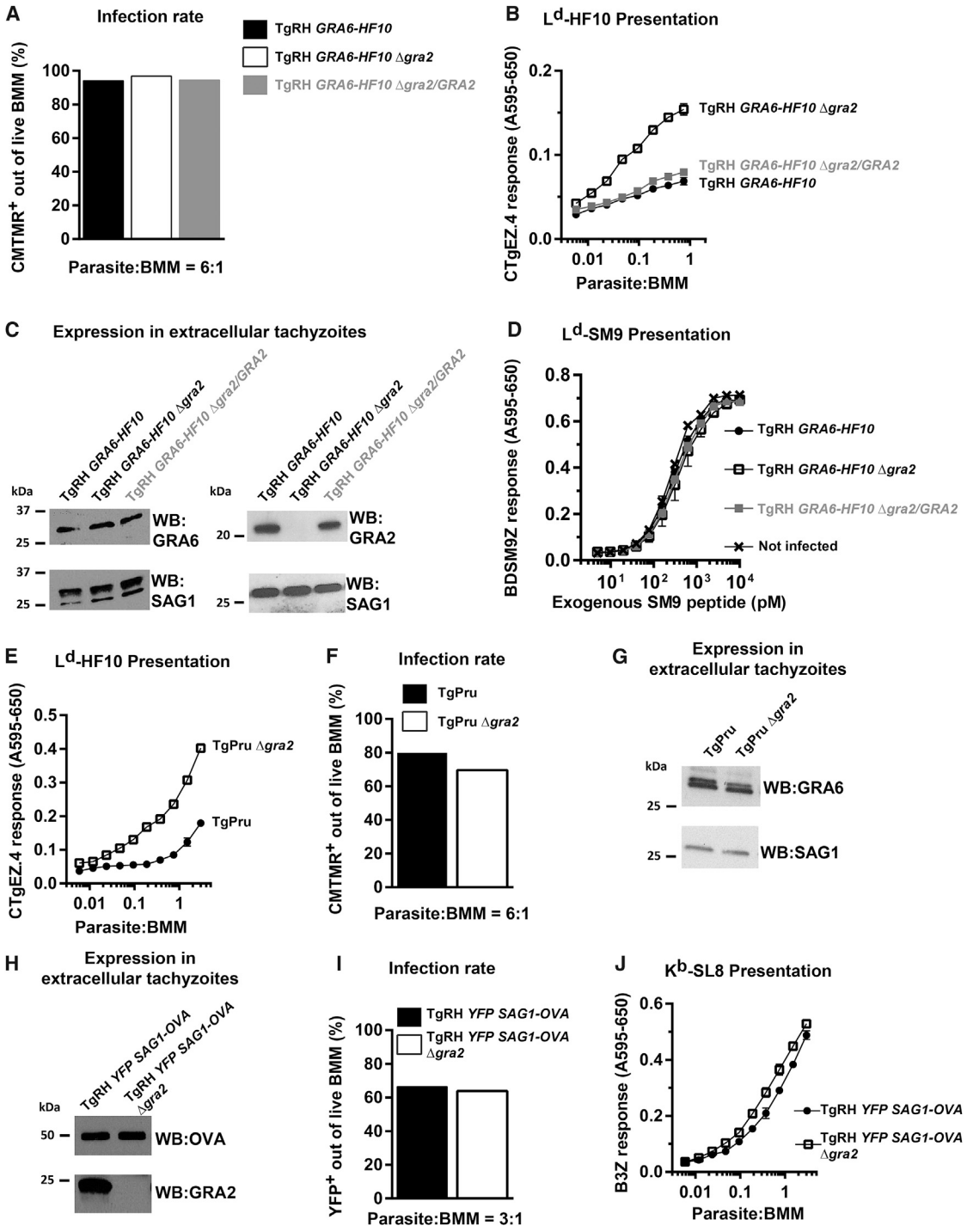

Figure 4. In Infected BMM, the IVN Decreases MHC Class I Presentation of the Membrane-Bound GRA6 Antigen

(A) Proportion of CMTMR$^+$ BMM (i.e., infected cells) out of live BMM measured 6 hr post-infection.

(B) L^d-HF10 presentation by BMM infected for 24 hr with the indicated parasites, assessed with the CTgEZ.4 hybridoma.

(C) Western blot (WB) analysis showing the expression level of GRA6 and GRA2 in the indicated parasite lines, with SAG1 as a loading control.

(D) Exogenous presentation of synthetic GRA4-derived SM9 peptide pulsed on BMM previously infected with the indicated parasites for 24 hr, assessed with the BDSM9Z hybridoma.

(E) L^d-HF10 presentation by BMM infected for 24 hr with TgPru or TgPru Δ*gra2*, assessed with the CTgEZ.4 hybridoma.

(F) Proportion of CMTMR$^+$ BMM (i.e., infected cells) out of live BMM measured 6 hr post-infection.

(legend continued on next page)

et al., 2008). Second, beyond antigen processing, our results suggest that membrane deformations (such as those forming the IVN) could be key determinants for controlling the passage of parasite proteins beyond the vacuolar boundary. Third, our work identifies additional parameters regulating immunogenicity of *T. gondii* antigens in the MHC class I pathway, an endeavor that will be crucial in improving the design of *T. gondii* as a vaccine vector.

Why does membrane binding enhance MHC class I presentation in the context of *T. gondii* infection? One could envisage two main hypotheses.

If anchored at the PV membrane with its C terminus exposed to the host cell cytosol, then the GRA6 C-terminal domain (which contains the HF10 epitope) could be cleaved and released into the cytosol by an endopeptidase before its final processing by the proteasome (Blanchard et al., 2008). Intriguingly, given the recently reported NFAT4 stimulatory activity of the GRA6 C terminus in type I *T. gondii* (Ma et al., 2014), such endopeptidase could also modulate the innate signals triggered by the GRA6 C-terminal domain. In both scenarios, the nature of the involved peptidase(s) is uncertain. Candidate enzymes include those known to generate MHC class I peptides in the cytosol; e.g., insulin-degrading enzyme (Parmentier et al., 2010), thimet oligopeptidase, or nardilysin (Kessler et al., 2011). Alternatively, given the transmembrane nature of GRA6, the C-terminal fragment may be released via intra-membrane proteolysis by enzymes of the rhomboid class. Testing the involvement of these proteases will first require us to determine the topology of GRA6 in the PV membrane and to assess the impact of its topology on presentation.

A second hypothesis to explain the higher immunogenicity of membrane-bound versus soluble antigens could be their closer proximity to a translocation machinery embedded within the PV membrane. Such a machinery could involve the Sec61-based translocon, a protein complex normally mediating ER-to-cytosol retrotranslocation during the ERAD pathway. Sec61 has, indeed, been reported to be recruited from the host ER onto the PV membrane and to facilitate vacuole-to-cytosol export of the soluble SAG1-OVA antigen (Goldszmid et al., 2009). The ERAD machinery recruitment to the PV seems dependent on the Sec22b SNARE protein (Cebrian et al., 2011), but the role of Sec22b on presentation of the membrane-bound GRA6 will have to be investigated. Characterization of the post-vacuolar export pathway(s) for this category of antigens represents an exciting challenge for the coming years.

Why is presentation impaired by the IVN? The IVN may trap the antigen away from a C terminus-cleaving enzyme and act by steric hindrance. Alternatively, the high membrane curvature and/or lipid composition of the IVN may alter the translocation activity of a membrane-embedded "translocon." Rather than being inert bystander components, membranes can regulate protein function, especially the activity of translocases (Van Voorst and De Kruijff, 2000). This tuning may be driven by altered lateral pressure leading to structural rearrangements (Cantor, 2002). For instance, the lipid composition of the surrounding membranes affects lateral pressure on membrane-anchored helices of the TAP transporter and modulates its peptide transport activity (Schölz et al., 2011). Even though the *T. gondii* translocon(s) remain(s) to be identified, our data are consistent with the notion that membrane deformations of the PV are key regulators of this machinery. It will be useful to test the impact of IVN deletion on the trafficking of exported *T. gondii* effectors (Bougdour et al., 2014), especially those known to be membrane bound.

To date, the parameters known to favor immunogenicity of *T. gondii* antigens are active secretion in cells infected by live parasites (Dupont et al., 2014; Gregg et al., 2011; Kwok et al., 2003), C-terminal position within the source antigen (Feliu et al., 2013), and dense-granule-mediated (as opposed to rhoptry-mediated) release (Grover et al., 2014). Additionally, some secreted effectors associated with the IVN or the PV membrane can regulate the MHC class I pathway (L.M.R., B.A.F., V. Cantillana, G.A. Taylor, and D.J.B., unpublished data). Our work identifies two parameters promoting immunogenicity: association with vacuolar membranes and absence of IVN. These findings could help harness more effectively the potential of *T. gondii* as a vaccine vector, especially in the anti-tumor vaccination context. In pioneering studies, an attenuated strain of *T. gondii* was shown to promote anti-tumor immunity largely due to its strong adjuvant effect (Baird et al., 2013a, 2013b). It will be important to test whether expressing tumor antigen(s) in *T. gondii*, in the most immunogenic context defined here, could boost specific anti-tumor T cell responses and potentiate rejection.

Remarkably, the IVN of *T. gondii* is not the only example of membranous tubular structures present at the interface between an intracellular pathogen and its host. During both their intra-hepatic and intra-erythrocytic cycles, *Plasmodium* parasites trigger the formation of an exomembranous network of tubules (called the tubovesicular network; TVN) irradiating from the PV in the infected cell. In contrast to *T. gondii*, the effectors controlling TVN biogenesis remain elusive, but its dynamical and morphological properties, both at the blood (Hanssen et al., 2010) and liver stages (Grützke et al., 2014), have been studied. The *Plasmodium* TVN is typically viewed as an exchange platform that could either promote export of parasite components to the host and/or facilitate lipid acquisition. Its potential role in MHC I presentation by infected hepatocytes remains to be investigated. Another example is the *Salmonella* bacteria, which induce the formation of long membranous tubules (called SIT for *Salmonella*-induced tubules) extending from the *Salmonella*-containing vacuole into

(G) Western blot analysis showing the expression level of GRA6 in the parental and GRA2-deficient TgPru parasites, revealed with the anti-HF10 antiserum and SAG1 as a loading control.
(H) Western blot analysis showing the expression level of SAG1-OVA and GRA2 in the parental and GRA2-deficient TgRH *YFP SAG1-OVA* tachyzoites, revealed with the anti-OVA and anti-GRA2 antibodies.
(I) Proportion of YFP^+ BMM (i.e., infected cells) out of live BMM measured 6 hr post-infection.
(J) K^b-SL8 presentation by BMM infected for 8 hr with the indicated parasites, assessed with the B3Z hybridoma.
Data indicate mean ± SD. Data depicted on all panels are representative of three to five independent experiments.

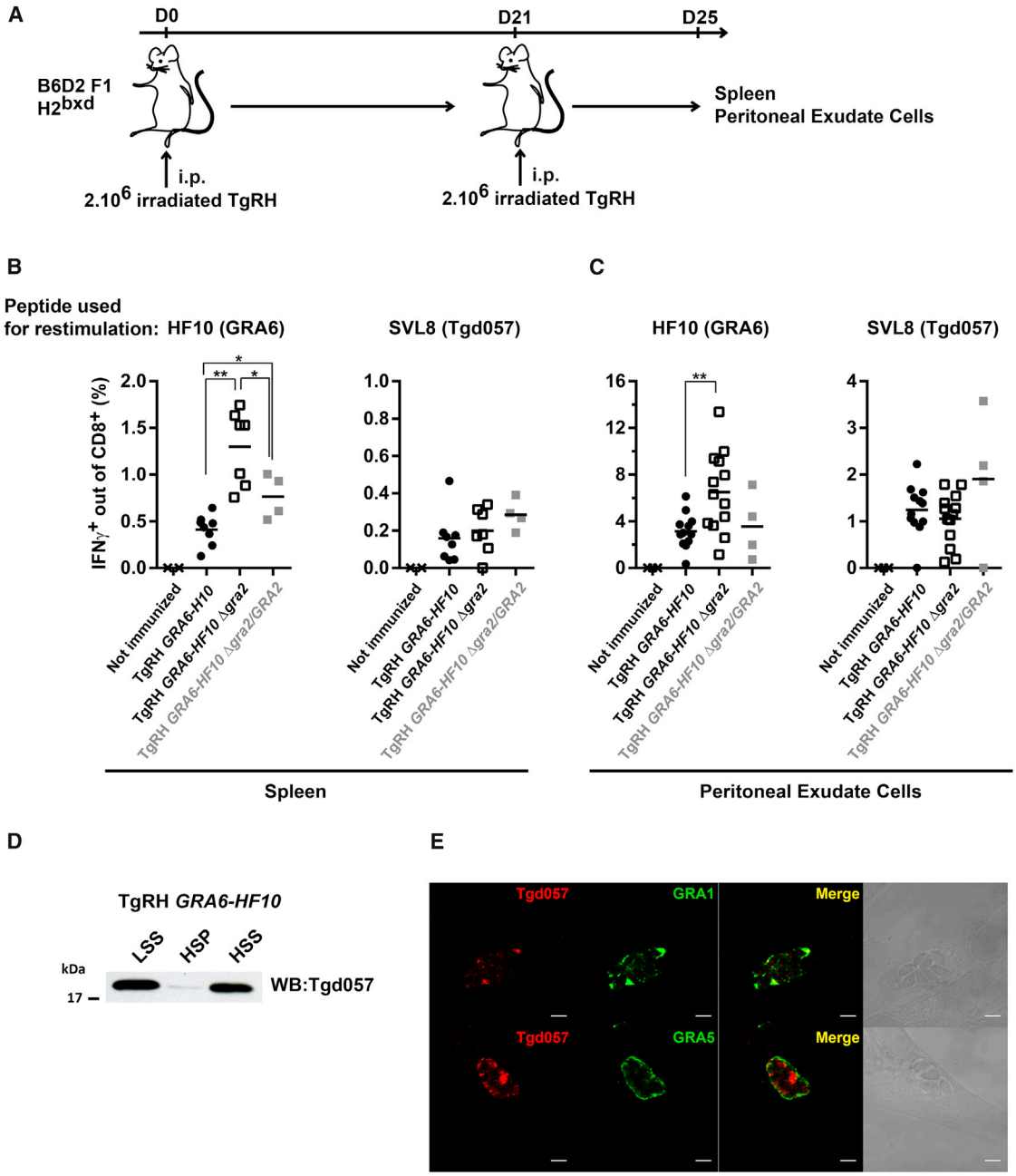

Figure 5. Immunization with *T. gondii* Devoid of IVN Enhances the T Cell Response to Membrane-Bound GRA6 but Does Not Affect the T Cell Response to Tgd057

(A) Description of the prime/boost immunization protocol and the ex vivo T cell response measurements. B6D2 F1 mice were immunized twice with irradiated TgRH *GRA6-HF10*, TgRH *GRA6-HF10* Δ*gra2*, or TgRH *GRA6-HF10* Δ*gra2*/*GRA2* parasites and analyzed 4 days after the second immunization. D, day.

(B and C) Ex vivo IFNγ intracellular staining of splenocytes (B) or peritoneal exudate cells (C) restimulated with the GRA6-derived HF10 or the Tgd057-derived SVL8 peptide. Bars represent the mean ± SEM. *$p < 0.05$; **$p < 0.005$. Data are pooled from two independent experiments.

(D) Solubility profile of endogenous Tgd057 in TgRH *GRA6-HF10* after mechanical disruption of overnight-infected HFF. Western blot (WB) analysis of Tgd057 present in LSS, HSP (insoluble, membrane bound), and HSS (soluble) fractions. Data are representative of three separate experiments.

(E) Subcellular localization of the endogenous Tgd057 protein in parallel with GRA1 (vacuolar lumen) and GRA5 (PV membrane) markers. Scale bars, 5 μm.

the host cell (Schroeder et al., 2011). SIT include at least three categories of tubules characterized by distinct morphologies and marker proteins (Krieger et al., 2014). Several effectors contributing to tubule biogenesis have been identified (Brumell et al., 2002), and the use of advanced imaging approaches has brought unprecedented insight on the ultrastructural morphology

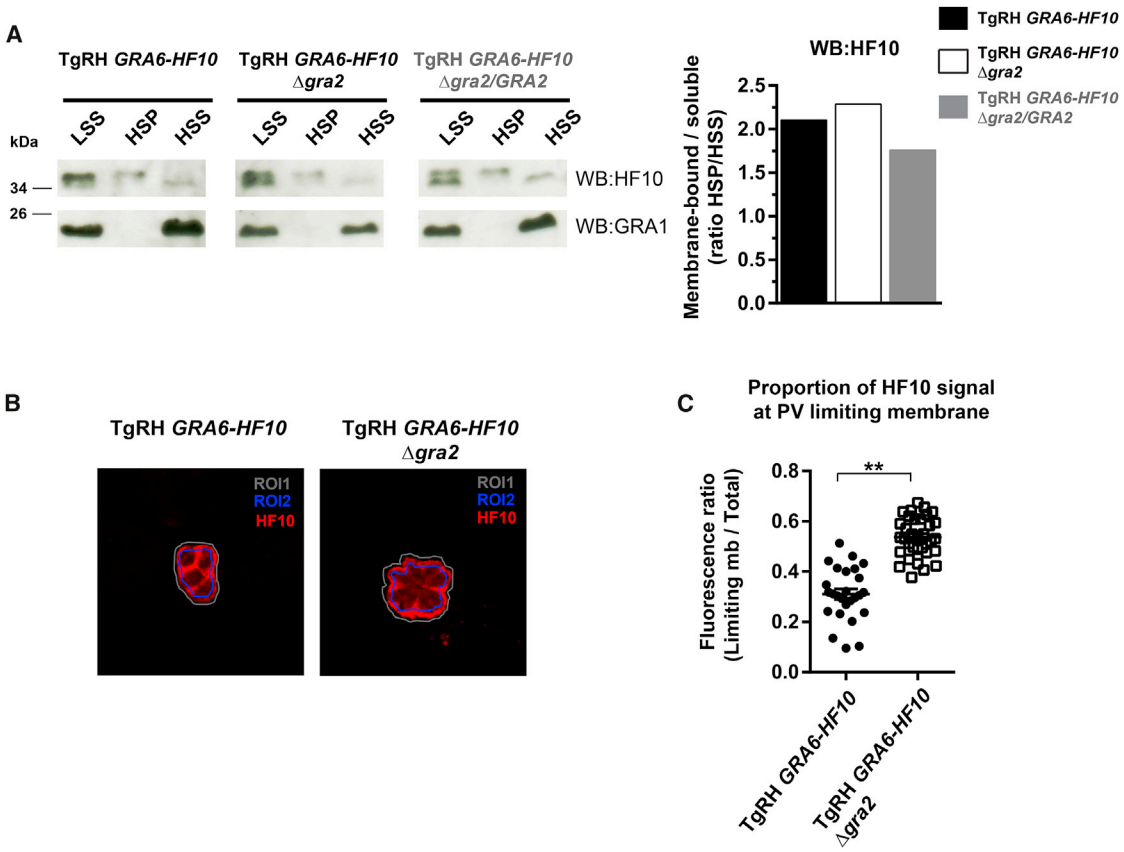

Figure 6. Disruption of the IVN Does Not Increase Solubility of the *T. gondii* Dominant Antigen GRA6 but Enhances Its Presence at the PV Membrane

(A) Solubility profile of GRA6-HF10, with or without GRA2. Western blot (WB) analysis of GRA6-HF10 present in LSS, HSP (insoluble, membrane bound), or HSS (soluble) fractions using the anti-HF10 antiserum. Histograms show the HSP over HSS ratio for one out of three experiments with similar results.

(B) Subcellular localization of GRA6-HF10 in HFF infected for 15 hr with TgRH *GRA6-HF10* or TgRH *GRA6-HF10* Δ*gra2* tachyzoites, visualized with the anti-HF10 antiserum. One confocal z section of a representative z stack is shown for each genotype. Gray indicates region of interest (ROI) 1, encompassing the entire PV; blue indicates ROI2, internal content.

(C) Proportion of HF10 fluorescence in the vicinity of the PV membrane (i.e., ROI1 minus ROI2) over the total HF10 fluorescence within the PV (i.e., ROI1). Each dot represents the median value of three ratio measurements, performed on three middle sections of a single PV. **$p < 0.005$. mb, membrane.

of SIT (Krieger et al., 2014). Formation of SIT correlates with bacteria intracellular fitness, but the precise benefit of these structures for the bacteria is uncertain, and whether they are involved in MHC class I presentation is unknown.

Several features distinguish the *Salmonella*, *T. gondii*, and *Plasmodium* membranous networks in terms of morphology, protein content, and dynamics. A major difference is that both the *Salmonella* SIT and the *Plasmodium* TVN are external with respect to the compartment in which the pathogen develops, while the *T. gondii* IVN is made of intravacuolar membranes. However, it is likely that findings in one system could inspire research on another pathogen and advance our understanding of these mysterious structures. Our present work suggests that the *T. gondii* IVN plays a role in immune modulation by interfering with the MHC class I pathway. These data pave the way for investigating how such membrane networks may influence antigen presentation in other intracellular pathogen infections.

EXPERIMENTAL PROCEDURES

Ethics Statement

Animal studies were carried out under the control of the National Veterinary Services and in accordance with the European Economic Community regulations (EEC directive 86/609, dated November 24, 1986). The protocol was approved by the Regional Ethics Committee of the Midi-Pyrénées Region (Approval MP/01/29/09/10).

Mice, Parasites, and Antibodies

C57BL/6JxDBA/2 F1 (B6D2) mice were purchased from Janvier and housed under specific pathogen-free conditions. Sex- and age-matched (8- to 12-week-old) mice were used. All parental and transgenic *T. gondii* strains used in this study were maintained by serial passages on confluent monolayers of human foreskin fibroblasts (HFF; ATCC SCRC-1041) and are listed in Table S1. Antibodies for flow cytometry were rat anti-CD8 (53-6.7) and mouse anti-IFN-γ (XMG1.2) (eBioscience). Primary antibodies for western blot and immunofluorescence were rabbit anti-Tgd057 serum and purified rabbit anti-HF10 serum (custom made, Biotem); rabbit anti-OVA (Sigma); and mouse monoclonal antibodies (mAbs) anti-SAG1 (TP3, Santa Cruz Biotechnology),

anti-GRA2 (TG17.179), anti-GRA1 (TG17.43), anti-GRA3 (T62H11), and anti-GRA5 (TG17.113)—the latter four produced by Biotem.

Plasmid Constructs and Parasite Transfection

Parasite transfections were performed as previously described (Feliu et al., 2013). The protocols used for the generation of each plasmid and parasite mutant are available in the Supplemental Experimental Procedures.

Western Blot and Subcellular Fractionation

Tachyzoites were released from infected HFF with a 23G needle and lysed with 1% Nonidet P-40 and protease inhibitors (cOmplete EDTA-free, Roche) for 30 min on ice. Lysates were centrifuged for 15 min at 15,000 × *g*. Proteins were reduced, separated by electrophoresis, and transferred to nitrocellulose membranes. Immunologic detection was performed using horseradish-peroxidase-conjugated antibodies (Promega) and quantified using a ChemiDoc system (Bio-Rad).

The solubility profile of GRA proteins within the PV was examined by cell fractionation of overnight-infected cells. Both the host cell and the PV membranes were mechanically disrupted by passing infected HFF through 25G needles, and released parasites were eliminated by a 2,000 × *g* centrifugation. The soluble fraction (high-speed supernatant; HSS) was separated from the membrane-associated fraction (high-speed pellet; HSP) by further centrifugation at 100,000 × *g* for 1 hr of the low-speed supernatant (LSS). Equal fractions of HSP and HSS were analyzed by immunoblot.

BMM and BMDC Differentiation and Antigen Presentation Assays

These experiments were performed as previously described (Feliu et al., 2013). Details can be found in the Supplemental Experimental Procedures.

Ex Vivo Analysis of T Cell Response

Mice were immunized twice 3 weeks apart with 2 × 10^6 tachyzoites that were previously γ-irradiated (120 Gy) and filtered through a 3-μm filter (Millipore). Mice were euthanized 4 days after the second immunization. Peritoneal exudate cells (PEC) were recovered by lavage with 10 ml cold PBS. Spleens were dissociated into single-cell suspensions in complete RPMI medium. Samples were depleted of erythrocytes, and production of IFN-γ was measured as described previously (Feliu et al., 2013). Samples were run on an FC500 (Beckman-Coulter) or a Fortessa (Becton Dickinson) flow cytometer and analyzed using the FlowJo software.

Immunofluorescence

Monolayers of HFF grown on Lab-Tek II chamber slides CC2 (Thermo Scientific Nunc) were infected with *T. gondii* for 16 to 24 hr. After infection, cells were washed with PBS, fixed for 20 min in 3% paraformaldehyde (Electron Microscopy Sciences) at room temperature (RT), and quenched for 5 min with PBS plus 0.1 M glycine. Primary antibodies were diluted in permeabilization buffer (PBS, 0.2% BSA, 0.05% saponin) and incubated for 1 hr at RT followed by three 5-min washes. Cells were incubated with AF555-coupled anti-rabbit immunoglobulin G (IgG) and AF633-coupled anti-mouse IgG (Invitrogen) for 20 min at RT. z stacks were acquired on a Zeiss LSM710 confocal microscope and analyzed using ImageJ software (NIH). For more details on the quantification of the GRA6 signal, see the Supplemental Experimental Procedures.

Lipid Extraction, Lipid Binding, and Tubulation Assays

Lipids were extracted from 10 × 150 cm^2 confluent flasks of HeLa cells (ATCC, CCL-2); glycerolipids were quantified after methanolysis, as previously described (Botté et al., 2008) and prepared as unilamellar vesicles, as detailed in the Supplemental Experimental Procedures. The protocols for detergent-free purification of rGRA2, rGRA2 ΔAAH, and rGRA6 proteins and their validation are described elsewhere (Bittame et al., 2015). For the protein-lipid overlay assays (fat blots), nitrocellulose membranes spotted with different lipids (100 pmol per spot) (Lipid Membrane Strips, Echelon Biosciences) were blocked for 1 hr with 3% fatty-acid-free BSA (FAF-BSA, Sigma-Aldrich) in TBS-T (Tris-buffered saline with 0.1% Tween 20) and incubated overnight at 4°C with 0.1 μg/ml of rGRA2 or rGRA2 ΔAAH diluted in TBS-T, 3% FAF-BSA. Following six washes in TBS-T, the proteins bound to lipids were revealed by immunoblot with specific antibodies against GRA2.

LUV-recombinant proteins incubation products were analyzed by flotation on a discontinuous sucrose gradient. Six micrograms of each recombinant protein were incubated for 30 min at RT with LUV formed from 160 μg of lipids, in 10 mM HEPES (pH 7.4), 150 mM NaCl. Sixty-five microliters of the binding mixture was mixed with 65 μl of 80% sucrose, loaded at the bottom of a 0.65-ml opened tube (Beckmann) and overlaid with five concentrations of sucrose (30% to 0%). Following a 100,000 × g centrifugation for 13 hr at 4°C, fractions were collected from the top of the gradient and analyzed by immunoblot. The phospholipids' unsaturated fatty acids were revealed by fumigation with iodine (Sigma-Aldrich).

For in vitro tubulation assays, 2–3 μl of each sample were adsorbed on the clean side of a carbon film that had been pre-evaporated on a mica sheet. The carbon film was detached from the mica by floating it in a well containing the negative stain solution. The carbon film was picked up onto a 400-mesh copper grid and air dried before observation with a JEOL 1200 EX II operating at 100 kV. All samples were stained with 2% (w/v) uranyl acetate. Images were recorded at the nominal magnifications of 10,000× or 40,000×.

Statistical Analyses

The Prism software (GraphPad) was used for statistical analyses. All p values were calculated with the two-tailed non-parametric Mann-Whitney test.

SUPPLEMENTAL INFORMATION

Supplemental Information includes Supplemental Experimental Procedures, seven figures, and one table and can be found with this article online at http://dx.doi.org/10.1016/j.celrep.2015.11.001.

AUTHOR CONTRIBUTIONS

Conceived and designed the experiments: N.B., J.L., C. Mercier, J.G., and M.-F.C.-D. Performed the experiments: J.L., A.B., C. Massera, J.G., C. Mercier, V.V., C.B., J.-F.D., G.E., and A.V. Analyzed the data: N.B., J.L., A.B., C. Massera, G.E., S.A., G.S., J.-F.D., J.G., C. Mercier, M.-F.C.-D., and W.W. Provided transgenic parasites: L.M.R., B.A.F., and D.J.B. Wrote the paper: N.B., J.L., and C. Mercier, with the help of all coauthors. M.-F.C.-D. and C. Mercier contributed equally.

ACKNOWLEDGMENTS

We thank the following: D. Soldati-Favre, P. Bradley, J. Boyle, and J. Boothroyd for reagents; G. van Dooren and B. Striepen for generating the TgRH *GRA6-HF10* parasites; E. Maréchal for quantification of fatty acid methyl esters; the CPTP flow cytometry and imaging core facilities; the INSERM UMS006-CREFRE animal care facility; the SCME Université de Montpellier 2; N.A. Guerrero, A. Lima-Perez, G. Pètre, L. Travier, P. Ruffiot, K. Sall, M. Jamin, E. Gentilhomme, and the N.B. team for help and discussions; D. Dunia and C. Bonnart for critical reading of the manuscript.

This work was supported by the Agence Nationale de la Recherche (ANR-11-BSV3-01002 to N.B. and M.-F.C.-D.); Région Midi-Pyrénées (N.B.); INSERM and Fondation Bettencourt-Schueller (Avenir Grant to N.B.); Human Frontier Science Program Organization (CDA00047/2011 to N.B.); a Marie Curie International Reintegration Grant (N.B.); the PIA Parafrap Consortium (ANR-11-LABX0024 to N.B. and M.-F.C.-D.); PIA Aninfimip equipment (ANR-11-EQPX-0003 to N.B.); a grant from Cluster 10 to Infectious Diseases-Rhône-Alpes region (C. Mercier); a PhD fellowship from the Rhône-Alpes region (A.B.); Fondation pour la Recherche Médicale (J.L.); NIH grants (AI091461, AI105593, AI108489) (D.J.B.); and a post-doctoral fellowship from the ANRS (G.E.). We acknowledge support from the platforms of the Grenoble Instruct Center (ISBG; UMS 3518 CNRS-CEA-UJF-EMBL) supported by the French Infrastructure for Integrated Structural Biology Initiative (FRISBI) (ANR-10-INSB-05-02) and GRAL (ANR-10-LABX-49-01) within the Grenoble Partnership for Structural Biology (PSB). W.W. is a member of the Institut Universitaire de France.

Received: March 11, 2015
Revised: August 11, 2015
Accepted: October 30, 2015
Published: November 25, 2015

REFERENCES

Baird, J.R., Byrne, K.T., Lizotte, P.H., Toraya-Brown, S., Scarlett, U.K., Alexander, M.P., Sheen, M.R., Fox, B.A., Bzik, D.J., Bosenberg, M., et al. (2013a). Immune-mediated regression of established B16F10 melanoma by intratumoral injection of attenuated Toxoplasma gondii protects against rechallenge. J. Immunol. *190*, 469–478.

Baird, J.R., Fox, B.A., Sanders, K.L., Lizotte, P.H., Cubillos-Ruiz, J.R., Scarlett, U.K., Rutkowski, M.R., Conejo-Garcia, J.R., Fiering, S., and Bzik, D.J. (2013b). Avirulent Toxoplasma gondii generates therapeutic antitumor immunity by reversing immunosuppression in the ovarian cancer microenvironment. Cancer Res. *73*, 3842–3851.

Bertholet, S., Goldszmid, R., Morrot, A., Debrabant, A., Afrin, F., Collazo-Custodio, C., Houde, M., Desjardins, M., Sher, A., and Sacks, D. (2006). Leishmania antigens are presented to CD8+ T cells by a transporter associated with antigen processing-independent pathway in vitro and in vivo. J. Immunol. *177*, 3525–3533.

Bittame, A., Effantin, G., Pètre, G., Ruffiot, P., Travier, L., Schoehn, G., Weissenhorn, W., Cesbron-Delauw, M.F., Gagnon, J., and Mercier, C. (2015). Toxoplasma gondii: biochemical and biophysical characterization of recombinant soluble dense granule proteins GRA2 and GRA6. Biochem. Biophys. Res. Commun. *459*, 107–112.

Blanchard, N., Gonzalez, F., Schaeffer, M., Joncker, N.T., Cheng, T., Shastri, A.J., Robey, E.A., and Shastri, N. (2008). Immunodominant, protective response to the parasite Toxoplasma gondii requires antigen processing in the endoplasmic reticulum. Nat. Immunol. *9*, 937–944.

Blum, J.S., Wearsch, P.A., and Cresswell, P. (2013). Pathways of antigen processing. Annu. Rev. Immunol. *31*, 443–473.

Botté, C., Saïdani, N., Mondragon, R., Mondragón, M., Isaac, G., Mui, E., McLeod, R., Dubremetz, J.F., Vial, H., Welti, R., et al. (2008). Subcellular localization and dynamics of a digalactolipid-like epitope in Toxoplasma gondii. J. Lipid Res. *49*, 746–762.

Bougdour, A., Tardieux, I., and Hakimi, M.A. (2014). Toxoplasma exports dense granule proteins beyond the vacuole to the host cell nucleus and rewires the host genome expression. Cell. Microbiol. *16*, 334–343.

Brumell, J.H., Goosney, D.L., and Finlay, B.B. (2002). SifA, a type III secreted effector of Salmonella typhimurium, directs Salmonella-induced filament (Sif) formation along microtubules. Traffic *3*, 407–415.

Cantor, R.S. (2002). Size distribution of barrel-stave aggregates of membrane peptides: influence of the bilayer lateral pressure profile. Biophys. J. *82*, 2520–2525.

Carruthers, V.B., and Sibley, L.D. (1997). Sequential protein secretion from three distinct organelles of Toxoplasma gondii accompanies invasion of human fibroblasts. Eur. J. Cell Biol. *73*, 114–123.

Cebrian, I., Visentin, G., Blanchard, N., Jouve, M., Bobard, A., Moita, C., Enninga, J., Moita, L.F., Amigorena, S., and Savina, A. (2011). Sec22b regulates phagosomal maturation and antigen crosspresentation by dendritic cells. Cell *147*, 1355–1368.

Cesbron-Delauw, M.F., Gendrin, C., Travier, L., Ruffiot, P., and Mercier, C. (2008). Apicomplexa in mammalian cells: trafficking to the parasitophorous vacuole. Traffic *9*, 657–664.

Dou, Z., McGovern, O.L., Di Cristina, M., and Carruthers, V.B. (2014). Toxoplasma gondii ingests and digests host cytosolic proteins. MBio *5*, e01188–e14.

Drin, G., and Antonny, B. (2010). Amphipathic helices and membrane curvature. FEBS Lett. *584*, 1840–1847.

Dupont, C.D., Christian, D.A., Selleck, E.M., Pepper, M., Leney-Greene, M., Harms Pritchard, G., Koshy, A.A., Wagage, S., Reuter, M.A., Sibley, L.D., et al. (2014). Parasite fate and involvement of infected cells in the induction of CD4+ and CD8+ T cell responses to Toxoplasma gondii. PLoS Pathog. *10*, e1004047.

Feliu, V., Vasseur, V., Grover, H.S., Chu, H.H., Brown, M.J., Wang, J., Boyle, J.P., Robey, E.A., Shastri, N., and Blanchard, N. (2013). Location of the CD8 T cell epitope within the antigenic precursor determines immunogenicity and protection against the Toxoplasma gondii parasite. PLoS Pathog. *9*, e1003449.

Fox, B.A., Falla, A., Rommereim, L.M., Tomita, T., Gigley, J.P., Mercier, C., Cesbron-Delauw, M.F., Weiss, L.M., and Bzik, D.J. (2011). Type II Toxoplasma gondii KU80 knockout strains enable functional analysis of genes required for cyst development and latent infection. Eukaryot. Cell *10*, 1193–1206.

Gendrin, C., Bittame, A., Mercier, C., and Cesbron-Delauw, M.F. (2010). Post-translational membrane sorting of the Toxoplasma gondii GRA6 protein into the parasite-containing vacuole is driven by its N-terminal domain. Int. J. Parasitol. *40*, 1325–1334.

Goldszmid, R.S., Coppens, I., Lev, A., Caspar, P., Mellman, I., and Sher, A. (2009). Host ER-parasitophorous vacuole interaction provides a route of entry for antigen cross-presentation in Toxoplasma gondii-infected dendritic cells. J. Exp. Med. *206*, 399–410.

Gregg, B., Dzierszinski, F., Tait, E., Jordan, K.A., Hunter, C.A., and Roos, D.S. (2011). Subcellular antigen location influences T-cell activation during acute infection with Toxoplasma gondii. PLoS ONE *6*, e22936.

Grover, H.S., Chu, H.H., Kelly, F.D., Yang, S.J., Reese, M.L., Blanchard, N., Gonzalez, F., Chan, S.W., Boothroyd, J.C., Shastri, N., and Robey, E.A. (2014). Impact of regulated secretion on antiparasitic CD8 T cell responses. Cell Rep. *7*, 1716–1728.

Grützke, J., Rindte, K., Goosmann, C., Silvie, O., Rauch, C., Heuer, D., Lehmann, M.J., Mueller, A.K., Brinkmann, V., Matuschewski, K., and Ingmundson, A. (2014). The spatiotemporal dynamics and membranous features of the Plasmodium liver stage tubovesicular network. Traffic *15*, 362–382.

Gubbels, M.J., Striepen, B., Shastri, N., Turkoz, M., and Robey, E.A. (2005). Class I major histocompatibility complex presentation of antigens that escape from the parasitophorous vacuole of Toxoplasma gondii. Infect. Immun. *73*, 703–711.

Hanssen, E., Carlton, P., Deed, S., Klonis, N., Sedat, J., DeRisi, J., and Tilley, L. (2010). Whole cell imaging reveals novel modular features of the exomembrane system of the malaria parasite, Plasmodium falciparum. Int. J. Parasitol. *40*, 123–134.

Kessler, J.H., Khan, S., Seifert, U., Le Gall, S., Chow, K.M., Paschen, A., Bres-Vloemans, S.A., de Ru, A., van Montfoort, N., Franken, K.L., et al. (2011). Antigen processing by nardilysin and thimet oligopeptidase generates cytotoxic T cell epitopes. Nat. Immunol. *12*, 45–53.

Kozlov, M.M., Campelo, F., Liska, N., Chernomordik, L.V., Marrink, S.J., and McMahon, H.T. (2014). Mechanisms shaping cell membranes. Curr. Opin. Cell Biol. *29*, 53–60.

Krieger, V., Liebl, D., Zhang, Y., Rajashekar, R., Chlanda, P., Giesker, K., Chikkaballi, D., and Hensel, M. (2014). Reorganization of the endosomal system in Salmonella-infected cells: the ultrastructure of Salmonella-induced tubular compartments. PLoS Pathog. *10*, e1004374.

Kwok, L.Y., Lütjen, S., Soltek, S., Soldati, D., Busch, D., Deckert, M., and Schlüter, D. (2003). The induction and kinetics of antigen-specific CD8 T cells are defined by the stage specificity and compartmentalization of the antigen in murine toxoplasmosis. J. Immunol. *170*, 1949–1957.

Labruyere, E., Lingnau, M., Mercier, C., and Sibley, L.D. (1999). Differential membrane targeting of the secretory proteins GRA4 and GRA6 within the parasitophorous vacuole formed by Toxoplasma gondii. Mol. Biochem. Parasitol. *102*, 311–324.

Lecordier, L., Moleon-Borodowsky, I., Dubremetz, J.F., Tourvieille, B., Mercier, C., Deslée, D., Capron, A., and Cesbron-Delauw, M.F. (1995). Characterization of a dense granule antigen of Toxoplasma gondii (GRA6) associated to the network of the parasitophorous vacuole. Mol. Biochem. Parasitol. *70*, 85–94.

Leriche, M.A., and Dubremetz, J.F. (1990). Exocytosis of Toxoplasma gondii dense granules into the parasitophorous vacuole after host cell invasion. Parasitol. Res. *76*, 559–562.

Ma, J.S., Sasai, M., Ohshima, J., Lee, Y., Bando, H., Takeda, K., and Yamamoto, M. (2014). Selective and strain-specific NFAT4 activation by the Toxoplasma gondii polymorphic dense granule protein GRA6. J. Exp. Med. *211*, 2013–2032.

Magno, R.C., Lemgruber, L., Vommaro, R.C., De Souza, W., and Attias, M. (2005). Intravacuolar network may act as a mechanical support for Toxoplasma gondii inside the parasitophorous vacuole. Microsc. Res. Tech. *67*, 45–52.

Mercier, C., Howe, D.K., Mordue, D., Lingnau, M., and Sibley, L.D. (1998). Targeted disruption of the GRA2 locus in Toxoplasma gondii decreases acute virulence in mice. Infect. Immun. *66*, 4176–4182.

Mercier, C., Dubremetz, J.F., Rauscher, B., Lecordier, L., Sibley, L.D., and Cesbron-Delauw, M.F. (2002). Biogenesis of nanotubular network in Toxoplasma parasitophorous vacuole induced by parasite proteins. Mol. Biol. Cell *13*, 2397–2409.

Niedelman, W., Gold, D.A., Rosowski, E.E., Sprokholt, J.K., Lim, D., Farid Arenas, A., Melo, M.B., Spooner, E., Yaffe, M.B., and Saeij, J.P. (2012). The rhoptry proteins ROP18 and ROP5 mediate Toxoplasma gondii evasion of the murine, but not the human, interferon-gamma response. PLoS Pathog. *8*, e1002784.

Parker, S.J., Roberts, C.W., and Alexander, J. (1991). CD8+ T cells are the major lymphocyte subpopulation involved in the protective immune response to Toxoplasma gondii in mice. Clin. Exp. Immunol. *84*, 207–212.

Parmentier, N., Stroobant, V., Colau, D., de Diesbach, P., Morel, S., Chapiro, J., van Endert, P., and Van den Eynde, B.J. (2010). Production of an antigenic peptide by insulin-degrading enzyme. Nat. Immunol. *11*, 449–454.

Phillips, R., Ursell, T., Wiggins, P., and Sens, P. (2009). Emerging roles for lipids in shaping membrane-protein function. Nature *459*, 379–385.

Schmick, M., and Bastiaens, P.I. (2014). The interdependence of membrane shape and cellular signal processing. Cell *156*, 1132–1138.

Schölz, C., Parcej, D., Ejsing, C.S., Robenek, H., Urbatsch, I.L., and Tampé, R. (2011). Specific lipids modulate the transporter associated with antigen processing (TAP). J. Biol. Chem. *286*, 13346–13356.

Schroeder, N., Mota, L.J., and Méresse, S. (2011). Salmonella-induced tubular networks. Trends Microbiol. *19*, 268–277.

Sibley, L.D. (2011). Invasion and intracellular survival by protozoan parasites. Immunol. Rev. *240*, 72–91.

Sibley, L.D., Niesman, I.R., Parmley, S.F., and Cesbron-Delauw, M.F. (1995). Regulated secretion of multi-lamellar vesicles leads to formation of a tubulovesicular network in host-cell vacuoles occupied by Toxoplasma gondii. J. Cell Sci. *108*, 1669–1677.

Suzuki, Y., and Remington, J.S. (1990). The effect of anti-IFN-gamma antibody on the protective effect of Lyt-2+ immune T cells against toxoplasmosis in mice. J. Immunol. *144*, 1954–1956.

Tonnesen, A., Christensen, S.M., Tkach, V., and Stamou, D. (2014). Geometrical membrane curvature as an allosteric regulator of membrane protein structure and function. Biophys. J. *106*, 201–209.

Travier, L., Mondragon, R., Dubremetz, J.F., Musset, K., Mondragon, M., Gonzalez, S., Cesbron-Delauw, M.F., and Mercier, C. (2008). Functional domains of the Toxoplasma GRA2 protein in the formation of the membranous nanotubular network of the parasitophorous vacuole. Int. J. Parasitol. *38*, 757–773.

Van Voorst, F., and De Kruijff, B. (2000). Role of lipids in the translocation of proteins across membranes. Biochem. J. *347*, 601–612.

Wilson, D.C., Grotenbreg, G.M., Liu, K., Zhao, Y., Frickel, E.M., Gubbels, M.J., Ploegh, H.L., and Yap, G.S. (2010). Differential regulation of effector- and central-memory responses to Toxoplasma gondii Infection by IL-12 revealed by tracking of Tgd057-specific CD8+ T cells. PLoS Pathog. *6*, e1000815.